SCIENTIFIC REPORTS

OPEN

SUBJECT AREAS:
NANOPHOTONICS AND PLASMONICS
SUB-WAVELENGTH OPTICS

Received
20 May 2014

Accepted
20 June 2014

Published
14 July 2014

Correspondence and requests for materials should be addressed to S.H.S. (shsong@hanyang.ac.kr)

Unified Theory of Surface-Plasmonic Enhancement and Extinction of Light Transmission through Metallic Nanoslit Arrays

Jae Woong Yoon[1], Jun Hyung Lee[2], Seok Ho Song[2] & Robert Magnusson[1]

[1]Dept. of Electrical Engineering, University of Texas at Arlington, Box 19016, Arlington, TX 76019, USA, [2]Dept. of Physics, Hanyang University, Seoul 133-791, KOREA.

Metallic nanostructures are of immense scientific interest owing to unexpectedly strong interaction with light in deep subwavelength scales. Resonant excitations of surface and cavity plasmonic modes mediate strong light localization in nanoscale objects. Nevertheless, the role of surface plasmon-polaritons (SPP) in light transmission through a simple one-dimensional system with metallic nanoslits has been the subject of longstanding debates. Here, we propose a unified theory that consistently explains the controversial effects of SPPs in metallic nanoslit arrays. We show that the SPPs excited on the entrance and exit interfaces induce near-total internal reflection and abrupt phase change of the slit-guided mode. These fundamental effects quantitatively describe positive and negative effects of SPP excitation in a self-consistent manner. Importantly, the theory shows excellent agreement with rigorous numerical calculations while providing profound physical insight into the properties of nanoplasmonic systems.

Renewed by the discovery of extraordinary optical transmission (EOT)[1,2], extensive study has been devoted to explaining light transmission through metal films with subwavelength aperture arrays. Initially, EOT through hole arrays was understood by local field enhancement with interfacial excitations evanescently coupled through subwavelength holes. Surface plasmon-polaritons (SPPs) in the optical domain[3–5] and geometrical surface resonances in the THz or microwave spectral ranges[6] induce such coupled interfacial excitations.

However, subwavelength slit arrays have shown many distinguished behaviors from those of hole arrays. A widely accepted enhancement mechanism for slit arrays is based on Fabry-Pérot resonances of slit-guided modes[7–18], i.e., cavity modes (CMs). Many recent papers conclude that CMs provide the enhancement mechanism while SPPs play only a negative role[13–16]. In this view that deters SPPs, spectral location of the transmission minimum corresponds to the SPP resonance condition and the associated field pattern shows typical SPP character with its null at the aperture opening. Strong surface-plasmonic absorption[15,16], excitation of a non-resonant SPP[13], and the surface-plasmonic bandgap effect[17,18] have been suggested explanations for these negative effects of SPPs. The negative effect of an SPP has also been reported for hole arrays, and different viewpoints based on the nonresonant SPP excitation[19] and destructive interference between transmission pathways via surface modes and hole-guided modes[20] have been published as suggested explanations.

Nevertheless, another bundle of recent papers have reported enhanced transmission with clear SPP characters in surface field patterns and frequency-dispersive properties[7–12]. In these analyses, SPPs enhance transmission with coexisting CMs[10–12]. Associated with SPP-CM hybrids, transmission peaks become much narrower than the pure CM resonances[8–10,12,17,18] — the CM resonance condition shifts abruptly[8,12] and an asymmetric Fano profile appears[21–23]. Therefore the role of SPPs in metallic nano aperture arrays is still under debate, and the essential physics remain unclear due to these diverging interpretations.

In this paper, we show that controversial SPP-related effects can be consistently described by a single unified model that treats a metallic nanoslit array as an optical cavity with SPP-resonant boundaries. We theoretically prove that all aforementioned SPP-related effects such as the antiresonant extinction, null field at the aperture opening, bandwidth narrowing, and abrupt shift of the CM resonance condition are rooted in a single resonance interaction: a surface-plasmonic Fano resonance that occurs when the external light and CM couple at the entrance and exit interfaces. Contributed by the SPP excitation, metal-film interfaces act as a Fano-resonant

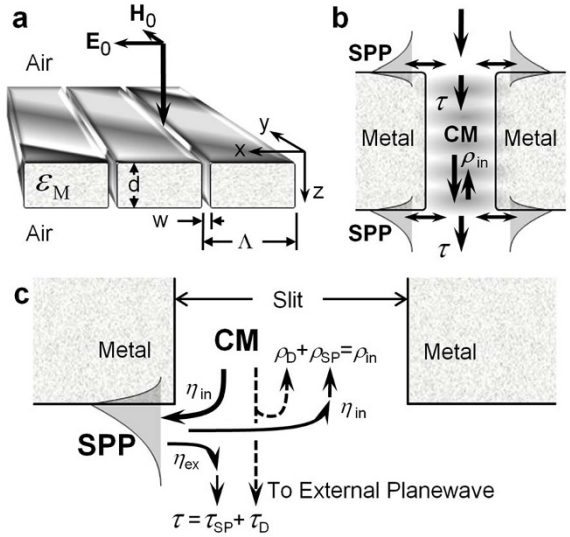

Figure 1 | Schematic of a surface-plasmonic Fano resonance model of a metallic nanoslit array. (a), Schematic of a one-dimensional array of metallic nanoslits. (b), Coupling of external light with the fundamental CM at the entrance and exit interfaces. τ represents the coupling coefficient between the external light and CM while ρ_{in} denotes the internal reflection coefficient of the CM. (c), Fano-resonance interpretation of the coupling between the external light and the CM at the single interface. ρ_{SP} and τ_{SP} represent reflection and transmission coefficients via an SPP state, respectively, while ρ_D and τ_D denote the nonresonant reflection and transmission amplitudes, respectively. η_{in} (η_{ex}) is the coupling probability of the SPP with the CM (external light).

gate that closes or opens nanoslit cavities and causes associated phase changes in the internal reflection of the CM. This interfacial interaction successfully describes various metamorphic SPP-related effects in a physically intuitive manner.

Analytic theory

Consider transmission of transverse-magnetic (TM) polarized light through a metal film perforated by an array of slits with period Λ, thickness d, and slit width w as shown in Fig. 1a. For deep subwavelength slits ($w \ll \lambda$) in an optically thick metal film ($d >$ skin depth $\lambda/2\pi|\varepsilon_M'|^{1/2}$), the light transmission can be described by a Fabry-Pérot formula for the fundamental CM[7,8,12,24,25] as

$$T = \left| \frac{\tau^2 e^{i\beta d}}{1 - \rho_{in}{}^2 e^{2i\beta d}} \right|^2, \quad (1)$$

where $\beta = \beta' + i\beta''$ is the complex propagation constant of the CM, τ is the coupling coefficient between the CM and external planewave, and ρ_{in} is the internal reflection coefficient of the CM as illustrated in Fig. 1b. Equation (1) is generally applicable to cases with arbitrary angles of incidence as long as only zero-order waves propagate in the surrounding media. Enhanced transmission peaks appear when the multiple scattering denominator in Eq. (1) becomes minimal at the phase-matching condition $\beta' d_q = (q + 1)\pi - \arg(\rho_{in})$, where q is an integer. The role of an SPP is implicitly held in τ and ρ_{in} as a mechanism causing a Fano resonance to occur at the top and bottom interfaces.

Here, we further examine the coupling processes at each film interface. We treat each interface as a Fano-resonant boundary where an SPP acts as a discrete state that interferes with the nonresonant continuum. In Fig. 1c, an SPP-resonant pathway interferes with a nonresonant pathway in the scattering processes of the incident CM. An SPP originally excited by the incident CM emits the reflected CM with probability η_{in} and the transmitted external radiation with probability η_{ex}. This process provides the resonant components of the single-interface reflection ρ_{SP} and transmission τ_{SP} coefficients. The incident CM at each interface also couples to the non-plasmonic reflection ρ_D and transmission τ_D. Using the optical Fano resonance theory developed by [22], the single-interface transmission τ and reflection ρ_{in} coefficients are written as

$$\tau(\delta) = \tau_D + \underbrace{\frac{2\sqrt{\eta_{in}\eta_{ex}}}{1 - i\delta} e^{i\phi}}_{=\tau_{SP}}, \quad (2)$$

$$\rho_{in}(\delta) = \rho_D + \underbrace{\frac{2\eta_{in}}{1 - i\delta} e^{i\varphi}}_{=\rho_{SP}}, \quad (3)$$

where $\delta = (\omega - \omega_{SP})/2\gamma_{tot}$ is the normalized frequency, ω_{SP} is the resonance frequency of the SPP, γ_{tot} is the total decay rate of the SPP, η_{in} and η_{ex} represent radiation probabilities of the SPP to the CM and the external planewave, respectively, ϕ is the plasmonic transmission phase at $\delta = 0$, and $\varphi = \arg(\rho_{SP})$ is the plasmonic reflection phase at $\delta = 0$. In this view to treat the interface responses, the time reversibility requirement dictates the phase differences between the plasmonic and non-plasmonic contributions, i.e., $\xi = \arg(\tau_D) - \arg(\tau_{SP})$ and $\zeta = \arg(\rho_D) - \arg(\rho_{SP})$ at $\delta = 0$, to be determined by[22]

$$e^{i\xi} = -\frac{\eta_{rad}|\tau_D|}{2\sqrt{\eta_{in}\eta_{ex}}} + i\sqrt{1 - \frac{\eta_{rad}{}^2|\tau_D|^2}{4\eta_{in}\eta_{ex}}}, \quad (4)$$

$$e^{i\zeta} = \frac{1}{|\rho_D|} + \left|\frac{\tau_D}{\rho_D}\right| \sqrt{\frac{\eta_{ex}}{\eta_{in}}} e^{i\xi}, \quad (5)$$

where $\eta_{rad} = \eta_{in} + \eta_{ex}$ is the total radiation probability of the SPP. Once establishing the real-valued parameters such as radiation probabilities (η_{in} and η_{ex}) and magnitudes of the nonresonant pathways ($|\rho_D|$ and $|\tau_D|$), we can describe the interference between the coupling pathways and the spectral properties of τ and ρ_{in} in a fully deterministic manner with these phase relations.

Lossless and nondispersive system

We check the theory with numerical calculation based on the rigorous coupled-wave analysis[26] (RCWA) and finite element method[27] (FEM). The metal is modeled by a complex dielectric constant $\varepsilon_M = \varepsilon_M' + i\varepsilon_M''$, where $\varepsilon_M' < 0$ and $\varepsilon_M'' \ll |\varepsilon_M'|$. Figures 2a and 2b show film-thickness-dependent transmission spectrum $T(\lambda,d)$ due to the RCWA and our analytic theory in Eqs (1) ~ (5), respectively. We assume here a lossless ($\varepsilon_M'' = 0$) metallic slit array with $\varepsilon_M = -5$ and slit width $w = 0.05\Lambda$ as an ideal case that reveals the essential physics with minimized complexity. We will discuss more realistic cases of lossy dispersive metals later in this paper. We extract the SPP resonance parameters ω_{SP}, γ, η_{in}, and η_{ex} for the analytic theory calculation from the single-interface SPP excitation spectrum calculated by FEM (see method section for details). We note that no numerical fitting method was used to find these parameters. Figures 2a and 2b confirm excellent quantitative agreement of periodically appearing CM Fabry-Pérot resonance peaks; more notably, the figures confirm drastic modification of CM resonance properties involving peak extinction at $\lambda/\Lambda = 1.13$ (red dashes) and an abrupt peak shift over the bright background region around $\lambda/\Lambda = 1.06$ (black dashes). These CM resonance modification effects are deeply associated with responses of the film interfaces and are therefore central to the controversy over the role of SPPs.

We analyze the response of the interface by assuming a semi-infinitely-thick slit array. Figure 2c shows the average intensity of the surface-normal electric field $|E_z|^2$ at the metal-air interface under planewave incidence from air (red squares) and CM incidence from slit (blue squares). The average $|E_z|^2$ spectra at the interface exhibit

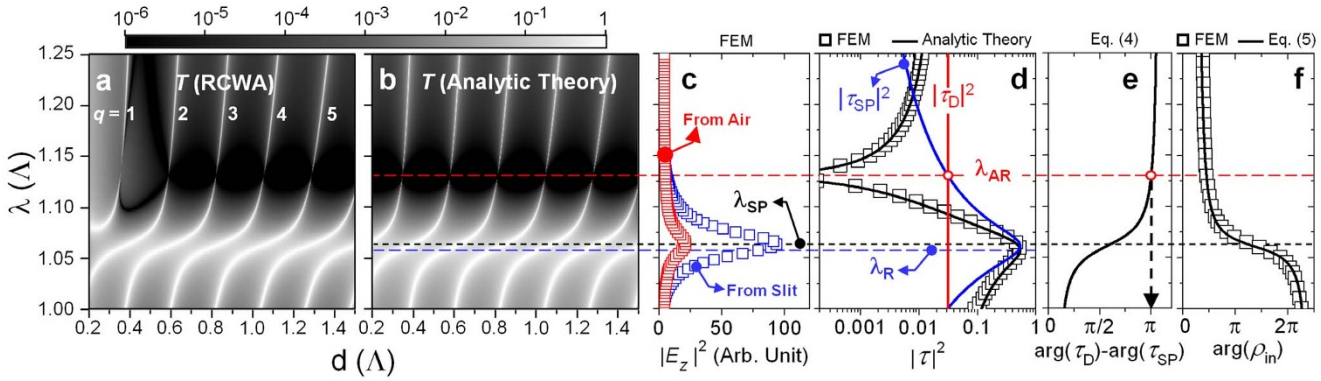

Figure 2 | Film transmittance *T* (a and b) vs. optical response of the single interface (c ~ f). Thickness-wavelength (λ-d) map of transmittance (*T*) through a finite film due to (a), RCWA and (b), the analytic theory. Note wavelength λ and film thickness d are in the unit of period Λ. (c), SPP excitation spectra ($|E_z|^2$ at the interface) for light incidence from air (red, □) and guided-mode incidence from slit (blue, □) on the single interface. (d), $|\tau|^2$ (black), $|\tau_{SP}|^2$ (blue), and $|\tau_D|^2$ (red) spectra. Open square symbols (□) are numerically calculated by FEM while curves (−) are obtained by the analytic theory. (e), Phase difference between τ_{SP} and τ_D due to Eq. (4). (f), Internal reflection phases arg(ρ_{in}) due to FEM (□) and Eq. (5) (−). $\varepsilon_M = -5$, w = 0.05Λ, and surface-normal incidence are assumed for all cases.

symmetric Lorentzian profiles with a common resonance center $\lambda_{SP} = 1.062\Lambda$ and full-width at half-maximum (FWHM) $\Delta\lambda_{SP} = 0.03211\Lambda$. We attribute this surface excitation to a pure SPP on a patterned surface. Using a pure-SPP model developed by Liu and Lalanne[5], we predict the SPP resonance wavelength and bandwidth (FWHM) on a metallic slit array to be

$$\lambda_{SP} = \frac{\lambda_{SPF}}{1 - \arg(t_S + r_S)/2\pi}, \tag{6}$$

$$\Delta\lambda_{SP} = \lambda_{SP}\left[\frac{\lambda_{SP}}{\pi\lambda_{SPF}}\ln\left(|t_S + r_S|^{-1}\right) + \frac{2n_{SP}''}{n_{SP}'}\right], \tag{7}$$

where t_S and r_S are in-plane SPP transmission and reflection coefficients at a single isolated slit, respectively, $\lambda_{SPF} = n_{SP}'\Lambda$ is the SPP resonance wavelength on a flat metal surface, and $n_{SP}' + n_{SP}'' = [\varepsilon_M/(1 + \varepsilon_M)]^{1/2}$ is the complex effective index of the SPP on a flat metal surface. FEM calculation of SPP scattering by a single isolated slit yields $\arg(t_S + r_S) = -0.1047\pi$ and $|t_S + r_S|^{-1} = 1.1097$. The SPP resonance wavelength and bandwidth due to Eqs. (6) and (7) are $\lambda_{SP} = 1.0624\Lambda$ and $\Delta\lambda_{SP} = 0.03346\Lambda$. These values quantitatively agree with those obtained from the surface excitation spectrum in Fig. 2c. See Supplementary Section I for the derivation of Eqs. (6) and (7) and Supplementary Section II for the FEM calculation of the in-plane SPP transmission t_S and reflection r_S coefficients.

The pure SPP excitation and associated Fano resonance at the interface successfully describe the drastic modification of CM resonance properties. The single-interface transmittance $|\tau|^2$ due to the analytic theory (solid curve −) in Fig. 2d shows excellent agreement with the numerical calculation result (square symbols □) due to FEM. A typical Fano resonance profile appears with its resonant enhancement peak at $\lambda_R = 1.058\Lambda$ ($<\lambda_{SP}$) and antiresonant extinction at $\lambda_{AR} = 1.130\Lambda$ ($>\lambda_{SP}$). First, the destructive interference between the plasmonic (τ_{SP}) and non-plasmonic (τ_D) coupling coefficients explains the antiresonant extinction of CM resonance peaks at λ_{AR}. Figure 2e shows the spectral behavior of the phase difference between τ_{SP} and τ_D, $\xi = \arg(\tau_D) - \arg(\tau_{SP})$ due to Eq. (4). Note at $\lambda = \lambda_{AR}$ the phase difference $\xi = \pi$ where $|\tau_{SP}| = |\tau_D|$ as shown in Fig. 2d, leading to complete destructive interference followed by $\tau = 0$. The null field at the slit opening for the excitation by external planewave in Fig. 3a is a natural consequence of the null excitation of the CM due to the complete destructive interference at λ_{AR}. In this interference description, the null field at the slit opening does not require any special electromagnetic excitation such as nonresonant SPP[13,19]. Note that in Fig. 3b the field at the slit opening is non-zero for the interface excitation by a CM at $\lambda = \lambda_{AR}$. The effect of the antiresonant extinction of τ on the film-transmittance *T* is obvious: the internal reflectance of the CM becomes total ($|\rho_{in}|^2 = 1 - |\tau|^2 \rightarrow 1$) as τ approaches 0. Therefore, the slits at $\lambda = \lambda_{AR}$ behave as closed cavities that generally support vanishingly narrow and extremely high-quality cavity resonance peaks.

On the other hand, at the SPP enhancement condition for $\lambda = \lambda_{SP}$ or λ_R, $|\tau|^2$ is maximal and consequently the slits behave as open cavities with partial transmission and reflection at the interface as shown in Figs. 3c and 3d. We note strong SPP excitation at the interface that leads to resonant phase change in the internal reflection of the CM. In Fig. 2f, the internal reflection phase arg(ρ_{in}) shows an S-shaped 2π change centered at $\lambda = \lambda_{SP}$. This phase behavior clearly describes the abrupt shift of the CM resonance peaks observed in Figs. 2a and 2b. Recalling the CM resonance condition $\beta' d_q = (q + 1)\pi - \arg(\rho_{in})$, 2π phase-change in ρ_{in} results in a transition of the resonant film thickness $d_q \rightarrow d_{q+2}$. This transition in the CM resonance condition is widely found in the literature[8,11,28] but has not been explained in terms of internal reflection phase change associated with the surface-plasmonic Fano resonance.

Lossy system

Now we consider the effect of material dissipation. Figures 4a and 4b show transmission spectra for several different film thicknesses (d/Λ = 1.03, 1.06, and 1.1) in lossless ($\varepsilon_M = -5$) and lossy ($\varepsilon_M = -5 + 0.01i$) cases, respectively. All solid curves calculated by the analytic theory in Eqs. (1) ~ (5) are again in excellent agreement with the RCWA simulation results (square symbols □). For the lossy case in Fig. 4b, the material dissipation is included in the analytic theory by including the non-radiative decay rate of the SPP $\gamma_{nr} = (2\pi c/\lambda_{SP})(n_{SP}''/n_{SP}')$ (see Supplementary Section I for details) and the complex propagation constant of the CM $\beta = \beta' + i\beta''$ that is given by the equation[29] $\varepsilon_M \tanh[w(\beta^2 - k_0^2)^{1/2}/2] = -[(\beta^2 - \varepsilon_M k_0^2)/(\beta^2 - k_0^2)]^{1/2}$, where $k_0 = 2\pi/\lambda$ and *c* is speed of light in vacuum.

The transmission peaks for $q = 4$ in Figs. 4a and 4b clearly reveal the effect of material absorption on the CM resonance peaks near the antiresonant extinction condition $\lambda = \lambda_{AR} = 1.130\Lambda$. For the lossless case in Fig. 4a, the linewidth of the transmission peak tends to vanish as the peak approaches λ_{AR}. Diverging CM localization lifetime in the closed cavity regime leads to an extremely narrow linewidth and a high local field enhancement. This is pointed out as the origin of the diverging inter-slit coupling matrix at the surface-mode resonance condition in the modal expansion method[2,9]. A transmission peak with an extremely narrow linewidth quickly disappears with material

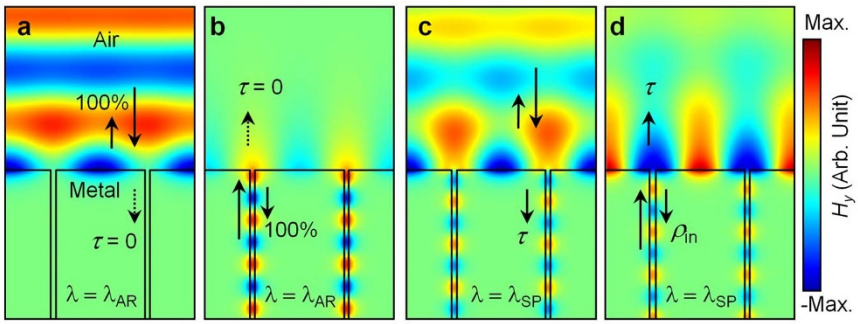

Figure 3 | Magnetic field (H_y) distributions for single interface excitation for (a), planewave incidence from air at the antiresonance condition ($\lambda = \lambda_{AR}$), and (b), guided-mode (CM) incidence from slit at $\lambda = \lambda_{AR}$, (c), planewave incidence from air at the SPP resonance center ($\lambda = \lambda_{SP}$), and (d), guided-mode (CM) incidence from slit at $\lambda = \lambda_{SP}$.

dissipation while those with a relatively wide linewidth near $\lambda = \lambda_{SP} = 1.062\Lambda$ or $\lambda_R = 1.058\Lambda$ are loss-insensitive as shown in Figs. 4a and 4b.

The relation between the peak transmittance (T_{max}) and the resonance quality factor Q, i.e., the number of effective oscillations in the cavity, quantitatively explains a narrow peak's high sensitivity to material dissipation. From Eq. (1) and the surface-plasmonic absorption $A_{SP} = 1 - |\tau|^2 - |\rho_{in}|^2$, we obtain $4\pi^2 T_{max} \approx Q^2|\tau|^2$ and $Q \approx 2\pi A_{SP}^{-1}\exp(-\beta'' d_q)$ in a high Q-factor regime ($Q \gg 1$). Whereas $T_{max} = 1$ in the lossless case, it decreases with Q^2 as ohmic damping of free electrons causes surface-plasmonic absorption (A_{SP}) at the interface and propagation loss of the CM (A_{CM}) inside the cavity. In Fig. 4c, the decrease in Q for the lossy case ($\varepsilon_M'' = 0.01$) is negligible near $\lambda = \lambda_{SP}$ or λ_R where Q is relatively small. In the extremely high Q band near λ_{AR}, however, Q is remarkably suppressed for the lossy case (red curve), resulting in strong suppression of T_{max} indicated by the gray curve enveloping the peaks in Fig. 4b. It is also worth noting that the surface-plasmonic absorption is not a dominant absorption channel responsible for the CM resonance extinction at λ_{AR}. The ratio of A_{SP} to A_{CM} in Fig. 4d is 0.1 at λ_{AR}, and thereby A_{CM} is nearly 10 times stronger than A_{SP}. In contrast, at $\lambda = \lambda_{SP} = 1.062\Lambda$ where surface-plasmonic absorption is maximized ($A_{SP}/A_{CM} = 7.44$), the effect of loss on Q and T_{max} is not remarkable as shown in Figs. 4b and 4c. Therefore, the propagation loss of a CM is dominantly responsible for the resonance extinction in this model system with $\varepsilon_M = -5 + 0.01i$.

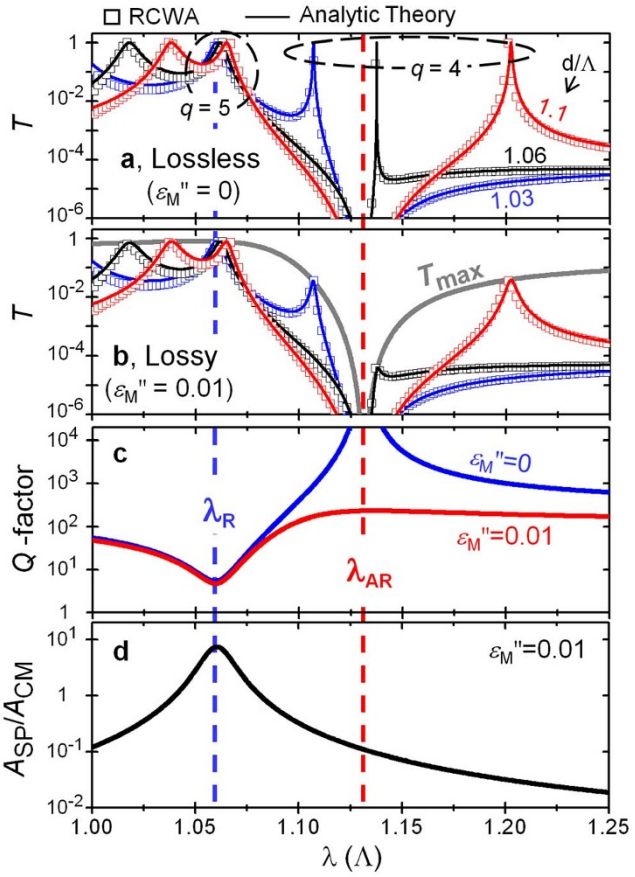

Figure 4 | **Effect of material dissipation on the film transmittance (T) and resonance quality factor.** The film transmittance (T) through (a), lossless ($\varepsilon_M'' = 0$) and (b), lossy ($\varepsilon_M'' = 0.01$) metal films for $d/\Lambda = 1.03$ (blue), 1.06 (black), and 1.1 (red). Square symbols (□) are obtained by RCWA simulation, and curves (−) represent the analytic theory based on Eqs. (1) ~ (5). (c), Resonance Q-factor spectra for $\varepsilon_M'' = 0$ (blue) and 0.01 (red). (d), Ratio of the SPP-induced absorption (A_{SP}) to the CM-induced absorption (A_{CM}) in a lossy metal film ($\varepsilon_M'' = 0.01$). $\lambda_R = 1.058\Lambda$ and $\lambda_{AR} = 1.130\Lambda$.

Lossy and dispersive system

In our description, λ_R, λ_{SP}, and λ_{AR} are crucial parameters strongly dependent on the metal dielectric constant ε_M. We use FEM to calculate λ_R, λ_{SP}, and λ_{AR} as a function of the real part ε_M' of ε_M, and the result is shown in Fig. 5. As ε_M' decreases to far negative values, λ_R

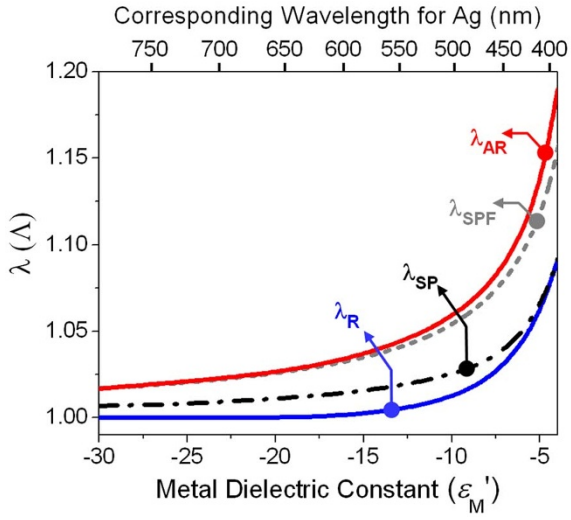

Figure 5 | **Dependence of characteristic wavelengths of the surface-plasmonic Fano resonance on metal dielectric constant (ε_M'):** the antiresonant extinction (λ_{AR}), SPP resonance center (λ_{SP}), resonant enhancement (λ_R), and SPP resonance center on a flat, unpatterned surface (λ_{SPF}). We assume slit width $w = 0.05\Lambda$.

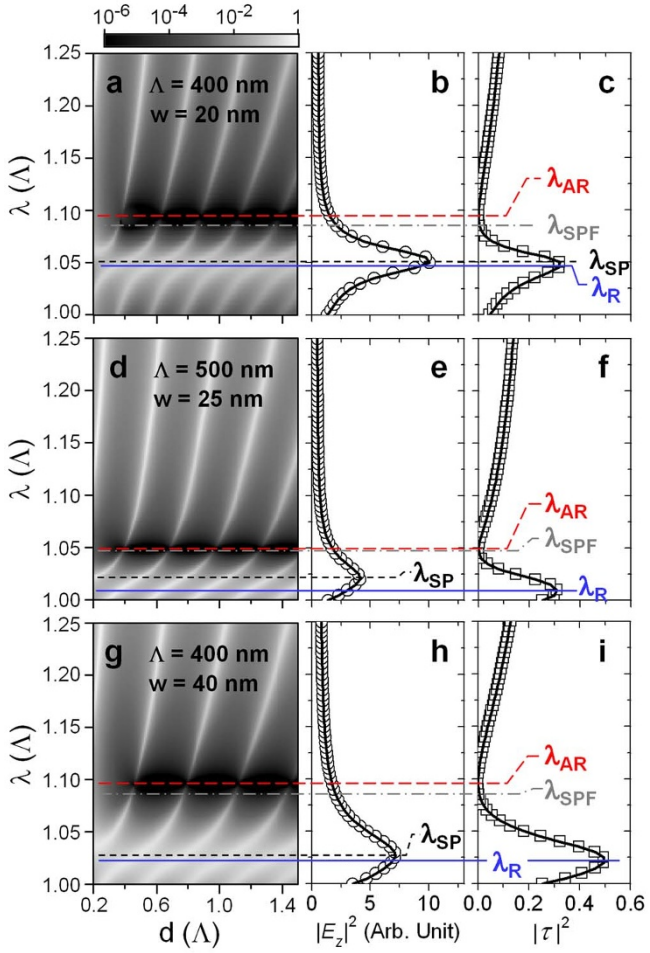

Figure 6 | Film-transmittance T (a, d, and g), surface excitation $|E_z|^2$ (b, e, and h), and single-interface transmittance $|\tau|^2$(c, f, and i) spectra for silver slit arrays: a, b, and c for period $\Lambda = 400$ nm and slit width w = 20 nm. d, e, and f for $\Lambda = 500$ nm and w = 25 nm. g, h, and i for $\Lambda = 400$ nm and w = 40 nm. We use the silver dielectric constant (ε_M) listed in [32]. Note that $|\tau|^2$ is on a linear scale, instead of the log scale used in Fig. 2d.

and λ_{AR} approach the canonical Rayleigh anomaly $\lambda_{Rayleigh} = \Lambda$ and the SPP resonance wavelength on a flat, unpatterned metal surface λ_{SPF}, respectively. Dependence of these characteristic locations on the metal dielectric constant (ε_M') suggests that previous confusion in the role of SPPs may originate from the spectral proximity of λ_R and λ_{AR} to $\lambda_{Rayleigh}$ and λ_{SPF}. For example, at $\varepsilon_M' \approx -15$ where many previous analyses have been performed[2], $|\lambda_{AR} - \lambda_{SPF}| \approx 4 \times 10^{-4}\Lambda$ and $|\lambda_R - \lambda_{Rayleigh}| \approx 1.5 \times 10^{-3}\Lambda$. In this situation, it is likely to form a hasty conclusion that the SPP plays only a negative role[15,16,30,31] and that the actual SPP-associated effects, such as the abrupt shift of the CM resonance condition, are confused with the effect of Rayleigh anomaly[28]. In [15,16] for example, the authors analyzed Au slit arrays in the near- and mid-infrared spectral domains where $\varepsilon_M' < -30$. Concluded by the coincidence of the antiresonant CM resonance extinction with the SPP resonance wavelength (λ_{SPF}) on a flat, unpatterned metal surface, they attribute the CM resonance extinction solely to the surface-plasmonic absorption. However, our model shows that an SPP induces high-Q CM resonances at the antiresonance condition, and the CM resonances in this case are highly sensitive to losses in any kind including both surface-plasmonic and cavity-modal absorption. Moreover, it is evident in Fig. 5 that the true SPP resonance wavelength λ_{SP} on a perforated metal surface differs from both λ_{SPF} and $\lambda_{Rayleigh}$ even down to $\varepsilon_M' \approx -30$, which corresponds to Ag for wavelength ~800 nm.

Finally, we show that all aspects of the simple Fano resonance model presented above are also present in realistic systems with lossy dispersive metals. In Fig. 6, we show the film-transmittance $T(\lambda,d)$, average field intensity $|E_z|^2$, and single-interface transmittance $|\tau(\lambda)|^2$ for silver nanoslit arrays with several different periods and slit widths. We use RCWA for $T(\lambda,d)$ and FEM for $|E_z|^2$ and $|\tau(\lambda)|^2$ with the realistic ε_M of silver experimentally obtained by Johnson and Christy[32]. For all three different cases, we confirm the same characteristic features as for the simplified case in Fig. 2; they include CM resonance modifications at $\lambda = \lambda_{SP}$ and λ_{AR} in $T(\lambda,d)$ associated with a single Lorentzian surface excitation in the $|E_z|^2$ spectrum and a typical Fano profile in $|\tau(\lambda)|^2$. In Figs. 6a ~ 6c for $\Lambda = 400$ nm and w = 20 nm, λ_{AR} is fairly separated from λ_{SPF} and resonance shift ($d_q \rightarrow d_{q+2}$) due to a 2π reflection-phase change that fully appears around λ_{SP}. In Figs. 6d ~ 6f for $\Lambda = 500$ nm and w = 25 nm, no additional feature appears. Affected by larger $|\varepsilon_M'|$ for the longer wavelength, λ_{AR} almost coincides with λ_{SPF} ($|\lambda_{AR} - \lambda_{SPF}| \sim 3 \times 10^{-3}\Lambda$) and the resonance shift near λ_R is seemingly associated with the Rayleigh anomaly at $\lambda = \Lambda$ as previously discussed in Fig. 5. In Figs. 6g ~ 6i for $\Lambda = 400$ nm and a wider slit width w = 40 nm, the wider slit results in a wide bandwidth in the SPP excitation. The Rayleigh anomaly, defined as sharp intensity variations occurring when an evanescent higher-order wave turns into a propagating wave, causes a corresponding decrease in the zero-order intensity. Our model is unable to describe effects associated with the Rayleigh anomaly because it is limited to a subwavelength-period regime where only the zero-order waves are allowed in the radiation continuum. Nevertheless, the rigorous calculation results for different cases in Figs. 1 and 6 consistently show no *necessary* effect of the Rayleigh anomaly on the resonance properties while the characteristic features of our interfacial Fano resonance model persistently appear. Therefore, the results in Figs. 1 and 6 suggest that the interfacial Fano resonance is the fundamental origin of the cavity resonance modification. In the previous literature, Sarrazin *et al.* reported a comprehensive spectral and surface field analysis also showing that the Rayleigh anomaly is unnecessary and they suggested the significance of surface-plasmonic Fano resonances with a phenomenological argument based on complex poles and zeros of scattering amplitudes[33].

We have shown that various aspects of SPPs in EOT through metallic nanoslit arrays can be consistently understood by the surface-plasmonic Fano resonance in the coupling of external radiation to the slit cavity mode. The Fano resonance interpretation was first suggested by Genet *et al.*[21] in order to explain the asymmetric profile and red shift of the enhanced transmission feature. They assumed a single discrete state without any other localized states such as a slit- or hole-guided mode. With detailed coupling processes unclear, the original Fano resonance interpretation has been used for phenomenological analyses of experimental and numerical data[2]. Our theory clearly describes where the Fano-type interference occurs, how it modifies the optical response of a metal surface with periodic nanoslits, and how the SPP-resonant metal surface finally contributes to metamorphic cavity-resonance properties.

Consistency with previous theories

In addition, our theory provides deeper physical insight into the microscopic theory of EOT developed by Liu and Lalanne[5]. For two-dimensional hole arrays, they found the single-interface transmission coefficient

$$\tau(\omega) = \tau_D + \frac{2ab}{\exp(-in_{SP}\omega\Lambda/c) - (t_S + r_S)} \qquad (8)$$

for normal incidence, where a and b denote coupling coefficients of an SPP with the hole-guided mode and external radiation, respectively. The Fano-type interference is an inevitable consequence of this expression as its first and second terms on the right-hand side

represent the nonresonant and resonant contributions, respectively. Equations (2) ~ (5) for Fano resonance in the single-interface coupling processes are applicable to two-dimensional hole arrays in principle. Therefore Eq. (8) should be consistent with our Fano resonance interpretation. Indeed, Eq. (8) reduces to Eq. (2) with radiation probabilities

$$\eta_{ex} = \frac{c}{|n_{SP}|\Lambda\gamma_{tot}}\frac{|b|^2}{|t_S + r_S|} \text{ and } \eta_{in} = \frac{c}{|n_{SP}|\Lambda\gamma_{tot}}\frac{|a|^2}{|t_S + r_S|}, \quad (9)$$

and resonant transmission phase

$$\phi = \arg(a) + \arg(b) - \arg(t_S + r_S) - \arg(n_{SP}). \quad (10)$$

In Eq. (9), the total decay rate $\gamma_{tot} = (\pi c/\lambda_{SP}^2)\,\Delta\lambda_{SP}$ with λ_{SP} and $\Delta\lambda_{SP}$ in Eqs. (6) and (7), respectively. See Supplementary Section III for detailed derivation. These relations describe how elementary scattering processes of electromagnetic fields at the metal-film interfaces are associated with the more fundamental wave kinematic effect of Fano resonances. The formal consistency of our model with the microscopic theory of EOT suggests further importance of the Fano resonance interaction in longer wavelength ranges beyond the visible domain. A series of theoretical[34,35] and experimental[36] analyses recently showed that an additional contribution from the quasi-cylindrical wave can also be described by the same elementary scattering coefficients a, b, t_S, and r_S of an SPP. In the near-infrared and longer wavelength domains, the quasi-cylindrical wave is known to significantly contribute to the resonances in periodic arrays of metallic nanoapertures[36,37].

Conclusions

In conclusion, we propose a surface-plasmonic Fano resonance theory of the light transmission through metallic nanoslit arrays. Importantly, seemingly paradoxical, metamorphic SPP-related effects are clearly explained by the pure surface-plasmonic Fano resonance effects at the film interfaces, which cause drastic modification of the cavity-resonances inside nanoslits. We also show that the interfacial Fano resonance interpretation is formally consistent with the microscopic theory of EOT through two-dimensional hole arrays. Therefore, for a two-dimensional array of large holes that allow propagating guided modes, a surface mode must lead to fundamentally the same effects on the cavity-mode resonance properties as those in one-dimensional slit arrays. For example, Catrysse and Fan[20] reported the antiresonant extinction of transmission peaks associated with hole-guided modes when the surface mode is resonantly excited in an SiC film with cylindrical holes. We believe that our theory unifies different interpretations and illuminates the origin of previous confusion regarding the role of SPPs. For example, the antiresonant extinction of CM resonance peaks is not simply a negative SPP effect but is rooted in the SPP-induced total internal reflection of the CM (SPP-induced cavity closing). Note that, in this case, the SPP actually contributes in a positive way as it leads to very high-Q CM resonances. Therefore, appropriate loss compensation methods[38,39] are of great interest at the antiresonant extinction condition as extremely high-Q nanocavity resonances are expected. We summarize how our theory unifies previous partial interpretations in Supplementary Table 1. Our model is limited to the zero-order regime and deep subwavelength slits that allow only the fundamental guided mode. Further development of our approach to more general cases of interfacial Fano resonance coupling with higher-order propagating waves and multiple localized modes may yield deeper physical insight into various nanophotonic and surface-plasmonic systems where interplay of coexisting modes induces versatile spectral properties and novel optical effects.

Methods

To estimate basic resonance parameters ω_{SP}, γ_{tot}, η_{in}, and η_{ex} for the analytic theory, we use surface excitation spectra in Fig. 2c. Two excitation spectra (red squares) for planewave incidence from air (blue squares) and for CM incidence from slit are denoted by E_{ex} and E_{in}, respectively. E_{ex} and E_{in} show Lorentzian resonance peaks with a common center and bandwidth. First, ω_{SP} and γ_{tot} are taken directly from the peak location and half-width at half-maximum of the Lorentzian profile. We obtain $\omega_{SP} = 0.9419 \times 2\pi c/\Lambda$ and $\gamma_{tot} = 0.02847 \times 2\pi c/\Lambda$ (c is speed of light in vacuum). Second, η_{in} and η_{ex} are taken from the peak values of E_{in} and E_{ex}. Considering Lorentz reciprocity theorem in the mode coupling processes, the radiation probability is proportional to the excitation probability. Therefore, $\eta_{in} \propto E_{in}(\lambda_{SP})$ and $\eta_{ex} \propto E_{ex}(\lambda_{SP})$. Including the relation for the total radiation probability $\eta_{in} + \eta_{ex} = \gamma_{rad}/\gamma_{tot}$, where γ_{rad} and γ_{tot} are radiation and total decay rate of the SPP mode, respectively, we obtain

$$\eta_{in} = \frac{E_{in}(\lambda_{SP})}{E_{in}(\lambda_{SP}) + E_{ex}(\lambda_{SP})}\frac{\gamma_{rad}}{\gamma_{tot}} \text{ and } \eta_{ex} = \frac{E_{ex}(\lambda_{SP})}{E_{in}(\lambda_{SP}) + E_{ex}(\lambda_{SP})}\frac{\gamma_{rad}}{\gamma_{tot}}.$$

The expressions for γ_{rad} and γ_{tot} are given in Supplementary Section I. Using these relations, we obtain $\eta_{in} = 0.1589$ and $\eta_{ex} = 0.8411$ from Fig. 2c. In this calculation, identical incoming power is assumed for the two different cases of external planewave incidence and CM incidence. In addition, $\gamma_{rad} = \gamma_{tot}$ in Fig. 2c as we assume lossless metal.

1. Ebbesen, T. W., Lezec, H. J., Ghaemi, H. F., Thio, T. & Wolff, P. A. Extraordinary optical transmission through sub-wavelength hole arrays. *Nautre* **391**, 667–669 (1998).
2. García-Vidal, F. J., Martín-Moreno, L., Ebbesen, T. W. & Kuipers, L. Light passing through subwavelength apertures. *Rev. Mod. Phys.* **82**, 729–787 (2010).
3. Martín-Moreno, L. *et al.* Theory of extraordinary optical transmission through subwavelength hole arrays. *Phys. Rev. Lett.* **86**, 1114–1117 (2001).
4. Barnes, W. L., Murray, W. A., Dintinger, J., Devaux, E. & Ebbesen, T. W. Surface plasmon polaritons and their role in the enhanced transmission of light through periodic arrays of subwavelength holes in a metal film. *Phys. Rev. Lett.* **92**, art. no.107401 (2004).
5. Liu, H. & Lalanne, P. Microscopic theory of the extraordinary optical transmission. *Nature* **452**, 728–731 (2008).
6. Pendry, J. B., Martín-Moreno, L. & García-Vidal, F. J. Mimicking surface plasmons with structured surfaces. *Science* **305**, 847–848 (2004).
7. Porto, J. A., García-Vidal, F. J. & Pendry, J. B. Transmission resonances on metallic gratings with very narrow slits. *Phys. Rev. Lett.* **83**, 2845–2848 (1999).
8. Ding, Y., Yoon, J., Javed, M. H., Song, S. H. & Magnusson, R. Mapping surface-plasmon polaritons and cavity modes in extraordinary optical transmission. *IEEE Photon. J.* **3**, 365–374 (2011).
9. García-Vidal, F. J. & L. Martín-Moreno, L. Transmission and focusing of light in one-dimensional periodically nanostructured metals. *Phys. Rev. B* **66**, art. no. 155412 (2002).
10. Marquier, F., Greffet, J. J. & Collin, S. Resonant transmission through a metallic film due to coupled modes. *Opt. Express* **13**, 70–76 (2005).
11. Guillaumée, M., Dunbar, L. A. & Stanley, R. P. Description of the modes governing the optical transmission through metal gratings. *Opt. Express* **19**, 4740–4755 (2011).
12. Sturman, B. & Podivilov, E. Theory of extraordinary light transmission through arrays of subwavelength slits. *Phys. Rev. B* **77**, art. no. 075106 (2008).
13. Lalanne, P., Sauvan, C., Hugonin, J. P., Rodier, J. C. & Chavel, P. Perturbative approach for surface plasmon effects on flat interfaces periodically corrugated by subwavelength apertures. *Phys. Rev. B* **68**, art. no. 125404 (2003).
14. Lin, L. & Roberts, A. Light transmission through nanostructured metallic films: coupling between surface waves and localized resonances. *Opt. Express* **19**, 2626–2633 (2011).
15. Lochbihler, H. & Depine, R. A. Properties of TM resonances on metallic slit gratings. *Appl. Opt.* **51**, 1729–1741 (2012).
16. Cao, Q. & Lalanne, P. Negative role of surface plasmons in the transmission of metallic gratings with very narrow slits. *Phys. Rev. Lett.* **88**, art. no. 057403 (2002).
17. Ceglia, D. de, Vincenti, M. A., Scalora, M., Akozbek, N. & Bloemer, M. J. Plasmonic band edge effects on the transmission properties of metal gratings. *AIP Advances* **1**, art. no. 032151 (2011).
18. D'Aguanno, G. *et al.* Transmission resonances in plasmonic metallic gratings. *J. Opt. Soc. Am. B* **28**, 253–264 (2011).
19. Maystre, D., Fehrembach, A.-L. & Popov, E. Plasmonic antiresonance through subwavelength hole arrays. *J. Opt. Soc. Am. A* **28**, 342–355 (2011).
20. Catrysse, P. B. & Fan, S. H. Propagating plasmonic mode in nanoscale apertures and its implications for extraordinary transmission. *J. Nanophotonics* **2**, art. no. 021790 (2008).
21. Genet, C., Exter, M. P. van. & Woerdman, J. P. Fano-type interpretation of red shifts and red tails in hole array transmission spectra. *Opt. Commun.* **225**, 331–336 (2003).
22. Yoon, J. W., Jung, M. J., Song, S. H. & Magnusson, R. Analytic theory of the resonance properties of metallic nanoslit arrays. *IEEE J. Quantum Electron.* **48**, 852–861 (2012).
23. Collin, S. *et al.* Nearly perfect Fano transmission resonances through nanoslits drilled in a metallic membrane. *Phys. Rev. Lett.* **104**, art. no. 027401 (2010).

24. Lalanne, P., Hugonin, J. P., Astilean, S., Palamaru, M. & Möller, K. D. One-mode model and Airy-like formulae for one-dimensional metallic gratings. *J. Opt. A Pure Appl. Opt.* **2**, 48–51 (2002).
25. Boyer, P. & Lebeke, D. van. Analytic study of resonance conditions in planar resonators. *J. Opt. Soc. Am. A* **29**, 1659–1666 (2012).
26. Moharam, M. G. & Gaylord, T. K. Rigorous coupled-wave analysis of planar-grating diffraction. *J. Opt. Soc. Amer.* **71**, 811–818 (1981).
27. Jin, J. *The finite element method in electromagnetics, 2nd Ed.* (John Wiley and Sons, New York, 2002).
28. Søndergaard, T. *et al.* Extraordinary optical transmission with tapered slits: effect of higher diffraction and slit resonance orders. *J. Opt. Soc. Am. B* **29**, 130–137 (2012).
29. Dionne, J. A., Sweatlock, L. A. & Atwater, H. A. Plasmon slot waveguides: Towards chip-scale propagation with subwavelength-scale localization. *Phys. Rev. B* **73**, art. no. 035407 (2006).
30. Weiner, J. The physics of light transmission through subwavelength apertures and aperture arrays. *Rep. Prog. Phys.* **72**, art. no. 064401 (2009).
31. Weiner, J. & Nunes, F. D. High-frequency response of subwavelength-structured metals in the petahertz domain. *Opt. Express* **16**, 21256–21270 (2008).
32. Johnson, P. B. & Christy, R. W. Optical constants of the noble metals. *Phys. Rev. B* **6**, 4370-4379 (1972).
33. Sarrazin, M., Vigneron, J.-P., & Vigoureux, J.-M. Role of Wood anomalies in optical properties of thin metallic films with a bidimensional array of subwavelength holes. *Phys. Rev. B* **67**, art. no. 085415 (2003).
34. Liu, H & Lalanne, P. Light scattering by metallic surfaces with subwavelength patterns. *Phys. Rev. B* **82**, art. no. 155418 (2010).
35. Liu, H. & Lalanne, P. Comprehensive microscopic model of the extraordinary optical transmission. *J. Opt. Soc. Am. A* **27**, 2542–2550 (2010).
36. Beijnum, F. van. *et al.* Quasi-cylindrical wave contribution in experiments on extraordinary optical transmission. *Nature* **492**, 411–414 (2012).
37. Lalanne, P. & Hugonin, J. P. Interaction between optical nano-objects at metallo-dielectric interfaces. *Nat. Phys.* **2**, 551–556 (2006).
38. Noginov, M. A. *et al.* Stimulated emission of surface plasmon polaritons. *Phys. Rev. Lett.* **101**, art. no.226806 (2008).
39. Leon, I. de & Berini, P. Amplification of long-range surface plasmons by a dipolar gain medium. *Nat. Photonics* **4**, 382–387 (2010).

Acknowledgments

The research leading to these results was supported in part by the Texas Instruments Distinguished University Chair in Nanoelectronics endowment and the National Research Foundation of Korea grant No. 2012R1A2A2A01018250 under the Korean Ministry of Education, Science and Technology.

Author contributions

This research was planned by J.W.Y., S.H.S. and R.M. J.W.Y. developed the analytic theory. Numerical simulation was performed by J.H.L. under supervision by S.H.S. and J.W.Y. The authors J.W.Y., J.H.L., S.H.S. and R.M. discussed the results. J.W.Y., S.H.S. and R.M. wrote the manuscript.

Additional information

Supplementary information accompanies this paper at http://www.nature.com/scientificreports

Competing financial interests: The authors declare no competing financial interests.

How to cite this article: Yoon, J.W., Lee, J.H., Song, S.H. & Magnusson, R. Unified Theory of Surface-Plasmonic Enhancement and Extinction of Light Transmission through Metallic Nanoslit Arrays. *Sci. Rep.* **4**, 5683; DOI:10.1038/srep05683 (2014).